Unconfined Lateral Diffusion and an Estimate of Pericellular Matrix Viscosity Revealed by Measuring the Mobility of Gold-tagged Lipids

Greta M. Lee, Fen Zhang, Akira Ishihara, Cheryl L. McNeil, and Ken A. Jacobson

Department of Cell Biology and Anatomy, University of North Carolina at Chapel Hill, Chapel Hill, North Carolina 27599

Abstract. Nanovid (video-enhanced) microscopy was used to determine whether lateral diffusion in the plasma membrane of colloidal gold–tagged lipid molecules is confined or is unrestricted. Confinement could be produced by domains within the plane of the plasma membrane or by filamentous barriers within the pericellular matrix. Fluorescein-phosphatidylethanolamine (Fl-PE), incorporated into the plasma membranes of cultured fibroblasts, epithelial cells and keratocytes, was labeled with 30-nm colloidal gold conjugated to anti-fluorescein (anti-Fl). The trajectories of the gold-labeled lipids were used to compute diffusion coefficients (D_G) and to test for restricted motion. On the cell lamella, the gold-labeled lipids diffused freely in the plasma membrane. Since the gold must move through the pericellular matrix as the attached lipid diffuses in the plasma membrane, this result suggests that any extensive filamentous barriers in the pericellular matrix are at least 40 nm from the plasma membrane surface. The average diffusion coefficients ranged from 1.1 to 1.7 $\times$ 10^{-9} cm^2/s. These values were lower than the average diffusion coefficients (D_F) (5.4 to 9.5 $\times$ 10^{-9} cm^2/s) obtained by FRAP. The lower D_G is partially due to the pericellular matrix as demonstrated by the result that heparinase treatment of keratocytes significantly increased D_G to 2.8 $\times$ 10^{-9} cm^2/s, but did not affect D_F. Pericellular matrix viscosity was estimated from the frictional coefficients computed from D_G and D_F and ranged from 0.5 to 0.9 poise for untreated cells. Heparinase treatment of keratocytes decreased the apparent viscosity to approximately 0.1 poise.

To evaluate the presence of domains or barriers, the trajectories and corresponding mean square displacement (MSD) plots of gold-labeled lipids were compared to the trajectories and MSD plots resulting from computer simulations of random walks within corrals. Based on these comparisons, we conclude that, if there are domains limiting the diffusion of Fl-PE, most are larger than 5 μm in diameter.

ALTHOUGH the fluidity of the plasma membrane is widely accepted, some types of molecules are thought to be restricted to or to be especially concentrated in small areas (for reviews see Curtain et al., 1988; Edidin, 1990). Obvious morphological domains exist in the form of gap junctions and the apical and basolateral surfaces of epithelial cells. Both protein-rich domains in fibroblasts (Edidin and Stroynowski, 1991; Yechiel and Edidin, 1987) and lipid-rich domains (Rodgers and Glaser, 1991; Yechiel and Edidin, 1987) have been reported. Discrete lipid phase transitions have been detected in sperm membranes by differential scanning calorimetry (Wolf et al., 1990). The presence and size of domains can be directly visualized in some cases (Rodgers and Glaser, 1991) or inferred from photobleaching measurements (Metcalf et al., 1986; Yechiel and Edidin, 1987) and laser trap experiments (Edidin et al., 1992).

Another direct approach for determining the presence and size of domains involves following the movements of individual molecules in the plasma membranes of living cells. This can be done with nanovid microscopy (Geerts et al., 1987) which uses 30- to 40-nm gold particles combined with video-enhanced contrast microscopy. Using this technique, DeBrabander et al. (1991) reported the presence of restricted motion for the Thy-1 molecule on 3T3 fibroblasts, but Kucik et al. (1990) found no indication of restricted motion on keratocytes using a Con A–labeled gold probe.

The interpretation of the movements of the gold-tagged molecules is complicated because the plasma membrane is not an isolated lipid bilayer with embedded proteins but has an associated pericellular matrix. The pericellular matrix, which can also be considered as the interface between the plasma membrane and the extracellular matrix (Hunziker et al., 1983; Hunziker and Schenk, 1987), is the site where the ectodomains of integral membrane glycoproteins, proteoglycans, and glycolipids intermingle with hyaluronan and a variety of extracellular matrix glycoproteins and proteoglycans (Hedman et al., 1992; Kjellen and Lindahl, 1991). The gold particle–ligand complex must move through this layer,

since most, if not all, cells have a pericellular matrix (Ito, 1974 and references therein). This matrix ranges in thickness from 50-nm to 20-μm thick, depending on cell type (Billings-Gagliardi et al., 1981; Underhill and Toole, 1982) and whether the hyaluronan-rich cell "coat" is considered part of the pericellular matrix (Knudson and Knudson, 1991; Toole, 1991). With the exception of highly specialized epithelial cells (Hartwig et al., 1987; Wade and Coleman, 1989) and red blood cells (Viitala and Jarnefelt, 1985), there is little known about the structure of the pericellular matrix. This lack of knowledge is partially due to the difficulty in preserving the matrix with conventional fixation (Hunziker and Schenk, 1987). Thus whether the pericellular matrix is sufficiently dense or interconnected so as to impede the motion of a 30- to 40-nm gold probe has not previously been explored.

In this study, we have asked whether gold-tagged lipid analogs exhibit confined or restricted diffusion in the plasma membrane of living cells. Confinement or restriction could occur because of in-plane membrane domains. Alternatively, or in addition, the structure of the pericellular matrix may form steric barriers reducing the lateral mobility of the gold probe. Thus, gold tagged lipids offer a novel way to probe both the lateral heterogeneity within the plane of the membrane and the structure of the pericellular matrix adjacent to the plasma membrane. We have previously characterized the movements of gold-labeled fluorescein phosphatidylethanolamine (Fl-PE)[1] in artificial membranes (Lee et al., 1991) and found that gold-labeled lipids diffuse freely in a planar membrane. We now show, that, in a variety of vertebrate cells, gold-labeled lipids can travel large distances in the plasma membrane. Thus, the gold–lipid complex is not restricted to moving within small, micron-sized plasma membrane domains, and the pericellular matrix is not so interconnected as to prevent free lateral motion of the gold-labeled lipids. However, the pericellular matrix did impede the lateral diffusion of the probe, suggesting that its structure exerted a viscous drag on the gold particle.

Materials and Methods

Cell Culture

Primary cultures of keratocytes were prepared from freshly removed goldfish scales. The scales were rinsed three times for 15 min each in Ham's F-12 Nutrient Mixture with 25 mM Hepes (Sigma Chemical Co., St. Louis, MO) plus 10% heat-inactivated FBS (TCM+) containing penicillin/streptomycin and fungizone. The scales were placed singly, cell side down, on 22 mm^2, No. 1, cleaned (as described in Lee et al., 1991) glass coverslips in 35-mm petri dishes in a moist chamber. Each scale was covered with a 12-mm round coverslip. After 15 min, 1 ml of TCM+ was added. The scale cultures were kept at room temperature in the moist chamber overnight. To dissociate sheets of cells which had migrated off the scale, the scale cultures were treated with PBS containing 1.0 mM Mg^{2+} (no Ca^{2+}) for 15 min and then were returned to TCM+. Fish scale fibroblasts were obtained by passage of the fish scale cultures after fibroblasts had overgrown the other cell types (in 1–2 wks). Fish scale fibroblasts were used in their third to fifth passage and 2 d after plating. PtK1 cells were maintained in TCM+ with gentamycin/kanamycin and C3H-10T1/2 cells were grown in Eagle's basal medium plus 25 mM Hepes (Sigma Chemical Co.) with 10% heat-inactivated FBS and gentamycin/kanamycin. PtK1 and C3H-10T1/2 cells were maintained at 37°C in a 7.5% CO_2 incubator and were also used the second day after plating on cleaned 22 mm^2, No. 1 glass coverslips.

Labeling of Cells

The cells were rinsed with TCM (no serum) for 1 to 2 min before adding 1 to 2 μg/ml Fl-PE (*N*-[5-fluorescein thiocarbamoyl]dipalmitoyl-L-alpha-phosphatidylethanolamine), Lot 9A (Molecular Probes, Inc., Eugene, OR) in TCM (prepared by adding 1 to 2 μl of 2 mg/ml stock solution in ethanol to 2 ml TCM while vortexing). The cells were incubated for 10 min with the Fl-PE in a moist chamber in the dark. For all labeling steps, the fish cultures were maintained at room temperature while PtK and C3H cells were maintained at 37°C. The cells were rinsed three times 2 min with TCM+, and then the coverslips were inverted over 100 μl of 30-nm gold anti-fluorescein(Fl) in TCM+ on a glass slide with two spacers cut from No. 2 glass coverslips. The gold anti-Fl was prepared and stored as previously described (Lee et al., 1991). The gold anti-Fl was washed three times in TCM+ before putting on the cells. After a 20-min incubation, unbound gold anti-Fl was washed out with 200 μl of TCM+, and the chamber was sealed with VALAP (1:1:2 by weight vaseline, lanolin, and paraffin). For FRAP measurements, all cells were labeled at room temperature using a four- to ten-fold higher concentration of Fl-PE.

Enzyme Treatment

For the heparinase treatment of keratocytes, 5 U of heparinase I from *Flavobacterium heparinum* (Sigma Chemical Co.) in PBS with Ca^{2+} and Mg^{2+} was put on the cells for 20 min at room temperature. The heparinase was removed and Fl-PE was added as above. For the PtK cells, heparinase (*Flavobacterium*) from Fluka Chemika-Biochemika (Ronkonkoma, NY) was used at approximately the same strength as for the keratocytes and the enzyme treatment was at 37°C.

Particle Exclusion Assay

This assay is used to delineate the pericellular matrix or cell coat of living cells (Goldberg and Toole, 1984; Knudson and Knudson, 1991). Horse red blood cells (MG Scientific, Buffalo Grove, IL) were washed in PBS and then fixed in 4% formaldehyde for 2 h. The erythrocytes were washed extensively in PBS before use. 100 μl of 1×10^{-8} cells/ml in PBS with 0.1% BSA was placed on a slide with spacers. A coverslip with cells was inverted over the red blood cells, and the chamber was sealed with VALAP. The slide was placed on the microscope and the erythrocytes were allowed to settle for 10 min before observation and photography.

Light Microscopy and Image Analysis

The instrumentation and procedure have previously been described in detail (Lee et al., 1991). Briefly, we used an Axiovert microscope (Carl Zeiss, Oberkochen, Germany) equipped with a 1.4 NA oil immersion condenser and a 1.3 NA, 100× Plan-Neofluar objective. A Hamamatsu C2400 newvicon camera was connected to the microscope with a 4× adapter. Brightfield microscopy was used for gold particle imaging and differential interference contrast microscopy was used to see cellular details. An Image-1 processor (Universal Imaging Corp., West Chester, PA) was used to digitally enhance, record, and analyze images. Images were stored on an optical memory disk recorder (Panasonic 2028F), usually in a series of 200 images at video rate (30 frames/s). Images were retrieved and further processed to improve the distinction between the gold and the background before locating the centroids of each gold particle in each image. The accuracy of locating the position of the centroid was limited to pixel size which was 50–60 nm at the magnification used. A tracking program (Lee et al., 1991) was used to compute the trajectories by locating the nearest centroid in each succeeding image. Mean square displacements (MSD) and lateral diffusion coefficients (D) were computed as previously described (Lee et al., 1991). For the crawling cells, velocity corrections were made on the MSD according to the formula:

$$MSD = 4Dt + v^2t^2 \quad (1)$$

where v is the velocity of the crawling cell. The velocity was determined from the centroid of the nuclear area at the beginning and ending time points. Alternatively, when the whole nucleus was not visible (some cells would not wholly fit on the monitor at the magnification used), the displacement of the leading edge of the nucleus was measured. The velocity for each cell was applied to the corresponding trajectories for that cell. This correc-

1. *Abbreviations used in this paper*: anti-Fl, anti-fluorescein; D, diffusion coefficient; Fl-PE, fluorescein phosphatidylethanolamine; MSD, mean square displacement.

tion had little to no effect on the value of D for each trajectory because D was computed from the slope of the MSD plot over the shorter time intervals where the plot was linear (Lee et al., 1991). The corrections occasionally generated negative numbers for the MSD for the longer time intervals; these numbers were deleted when averaging the MSD's across trajectories and overall had little effect on the shape of the MSD plot and no effect on the value of D_G.

FRAP after Photobleaching

FRAP was used to obtain the D of the Fl-PE in the cell membranes independent of the gold tag. The instrumentation and procedure for FRAP has been previously described (Lee et al., 1991; Zhang et al., 1991). An oil immersion, 1.3 NA, 40× objective was used to bleach a 2.2-μm diam ($1/e^2$ width) spot.

Computer Simulations of Corralled Diffusion

The method for simulating two-dimensional random diffusion (Lee et al., 1991) was modified by creating a circular, impenetrable boundary around the domain. The size of the domain could be varied by adjusting the diameter of the boundary. The particle started at a random location within the circle and moved by steps in random directions. The step size was determined by the diffusion coefficient. The boundary was a non-reflective barrier. Thus a particle moving within the boundary would not be able to take a step which moved it over the boundary, but the clock would be incremented. No motion would be allowed until a step occurred in a direction which would move the particle to a new position inside the boundary region.

EM

Whole Mount. Cells were plated on formvar-coated gold locater grids attached to coverslips essentially as described (van den Pol, 1989). The cells were labeled as above and then fixed for 10 min in 3% glutaraldehyde in PBS containing 5 mM Mg^{2+} at room temperature. Video micrographs were made of selected cells. (There was no movement of the gold on the fixed cells.) With the grids still attached to the coverslips, the cells were postfixed in 0.5% OsO_4 0.8% $K_3Fe(CN)_6$ in PBS plus Mg^{2+} for 5 min at room temperature. After dehydration through increasing concentrations of ethanol and critical point drying, the grids were removed from the coverslips and the cells were examined on a JEOL transmission electron microscope. (A better method needs to be devised for removing the grids for the coverslips as this frequently resulted in cells with breaks in the cytoplasm.)

Sectioned Cells. Cells were grown in Lab-tek chambers with Permanox slides and labeled as above. After fixation in 2% glutaraldehyde containing 1% Alcian blue (Eastman Kodak, Co., Rochester, NY; Behnke and Zelander, 1970) in 0.1 M cacodylate buffer, pH 7, for 20 min at room temperature, the microchamber was removed from the slide containing the cells. The slide was inverted in buffer in a petri dish so that the cells would not be exposed to air or surface tension during subsequent solution changes. The cells were postfixed in 1% OsO_4 in cacodylate buffer for 60 min at room temperature. After embedding in epoxy resin, individual cells were selected and then sectioned perpendicular to the substrate. 60- to 70-nm sections were stained in 4% aqueous uranyl acetate for 20 min followed by 0.4% lead citrate for 8 min.

Results

Single 30-nm gold particles were present and detectable with our light microscope-image processing system. As shown in Fig. 1, several single gold particles are present in both the video and electron micrographs. The single gold particles are more readily detectable in the video image which has been further processed to allow automatic detection of the gold (Fig. 1 *B*). Not all of the single gold particles in the electron micrograph show up in the video image. Due to irregularities in the cell surface and the shallow depth of field of the high numerical aperture, 100× objective, all of the gold particles were not in the same focal plane with the light microscope. The majority of the gold particles were single: of more than 1,000 anti-Fl gold particles in electron micrographs of whole-mount preparations of PtK cells, 81% were single, 12% doublets, 4% triplets, and the remaining 2–3% were aggregates.

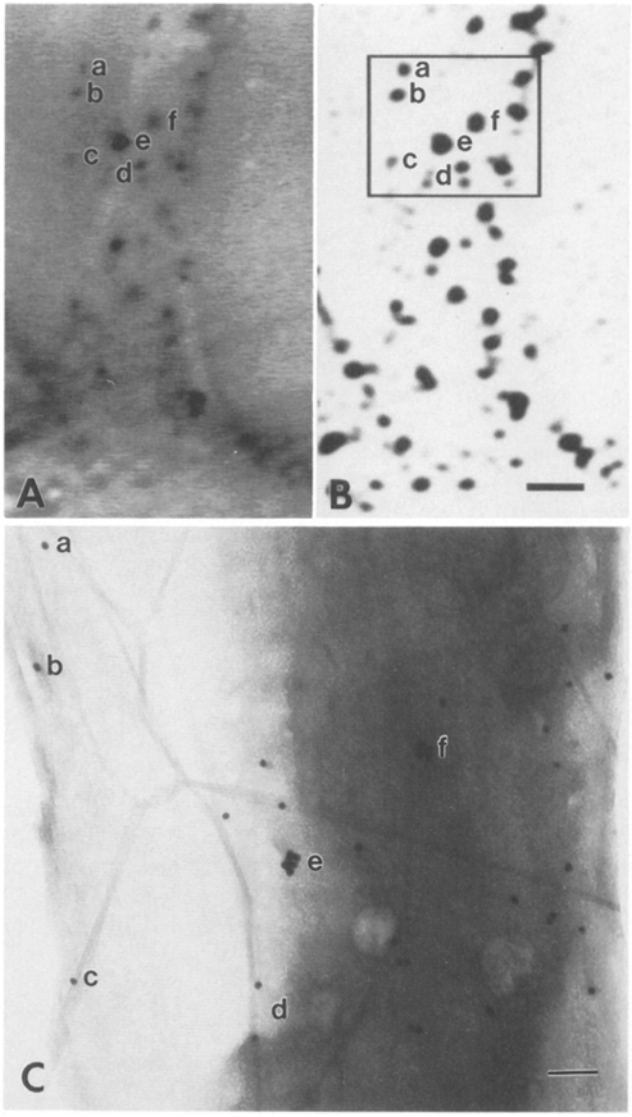

Figure 1. Brightfield video image of a region of a gold-labeled cell before (*A*) and after image processing for automatic detection of gold particles (*B*). The electron micrograph (*C*) of the boxed region in *B* demonstrates that individual 30-nm gold particles can be detected with our video microscope system. The lower case letters indicate corresponding single gold particles (*a–d*) and aggregates (*e* and *f*). This C3H fibroblast was labeled with 30 nm gold anti-pgp-1, which binds to an integral membrane glycoprotein. After fixation and imaging by nanovid microscopy, the cell was processed for whole-mount EM. The distances between the gold particles are shorter in the electron micrograph than in the video images due to cell shrinkage during the dehydration steps. Bars: (*B*) 2 μm; (*C*) 0.2 μm.

With brightfield microscopy, most cellular details are not visible but the gold is distinctly visible (Fig. 1). However, some organelles and highly ruffled areas have enough contrast to make automatic detection of the gold particles difficult. For this reason, spreading and locomoting cells were selected as they had large flat lamellae with few organelles. The lamella was used for most of the experiments presented here. The sloped perinuclear region which contains many or-

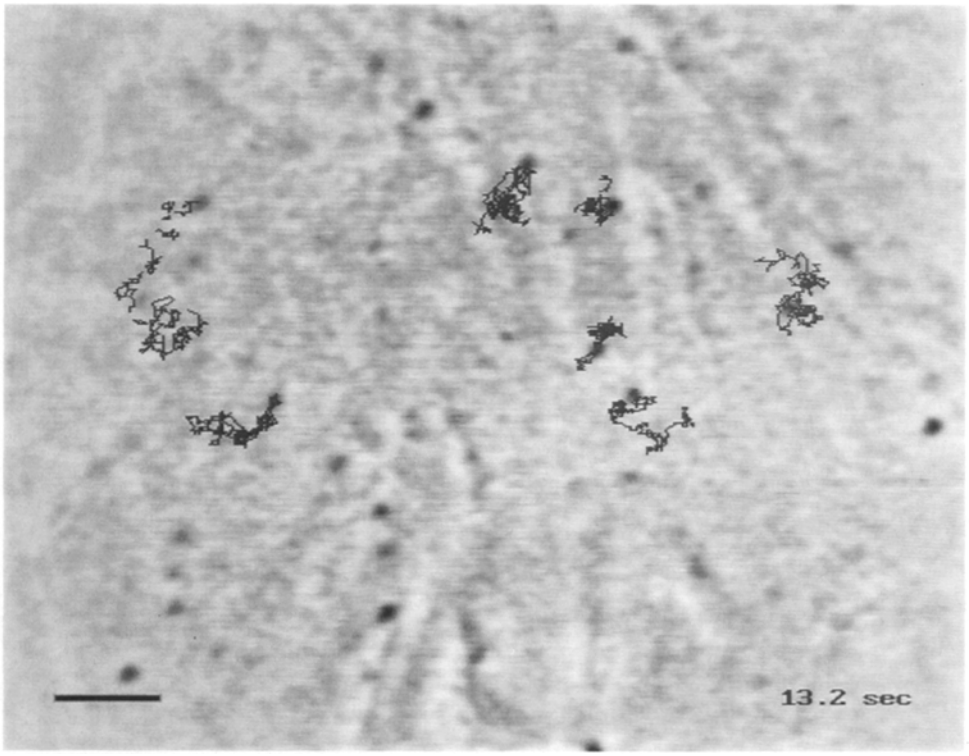

Figure 2. Gold tagged lipids move randomly in the plasma membrane of living cells. In this video-enhanced, bright-field image of the lamella of a C3H fibroblast the trajectories of some of the gold particles are shown superimposed on the cell. The particles were tracked for 13.2 s. For the trajectories shown, D ranges from 3×10^{-10} cm²/s to 1.5×10^{-9} cm²/s. Bar, 3 μm.

ganelles was avoided. The area of the plasma membrane over the nucleus could only be examined in those cells with a somewhat flat nucleus where most of this area could be in focus at the same time.

Gold-labeled lipids moved on the cell surface by Brownian motion as can be seen in the sample trajectories shown in Fig. 2. The trajectories, which were computed for 400 images collected at video rate (30 frames per second), show no consistent pattern or direction of motion, and the net displacement is highly variable. On the lamella, the average D

Table I. Comparison of D by Nanovid and FRAP for Fl-PE in Different Cell Types

Location	Nanovid microscopy		FRAP		
	$D_G \times 10^{-9}$ cm²/s	Percent particles w $D_G < 0.4 \times 10^{-9}$ cm²/s	$D_F \times 10^{-9}$ cm²/s	Immobile fraction (%)	D_G/D_F
Planar membrane‖					
multivalent gold	3.3 ± 2.9(74)*	30	13.3 ± 3.3(28)‡	30	0.25
paucivalent gold	7.6 ± 4.6(19)	16	13.3 ± 3.3(28)	30	0.57
Fibroblast (C3H)					
lamella	1.2 ± 0.7(58)	23	5.4 ± 2.7(30)	31	0.22
nuclear	1.3 ± 1.1(5)	71	3.8 ± 1.8(28)	29	0.34
PtK1					
lamella	1.1 ± 0.7(61)	13	6.3 ± 1.3(43)	29	0.17
+heparinase	1.4 ± 0.7(51)	21	–	–	–
Fish scale fibroblast					
lamella	1.7 ± 0.9(42)	14	9.5 ± 1.7(38)	26	0.18
Keratocyte, stationary					
lamella	1.4 ± 0.9(22)	15	6.2 ± 2.4(34)	36	0.22
+heparinase	2.5 ± 1.2(22)	–	6.6 ± 2.2(40)	34	0.38
Keratocyte, crawling					
lamella	1.3 ± 0.7(41)	20	–	–	–
+heparinase	2.8 ± 1.5(29)	0	–	–	0.42§

* Mean ± SD for gold-labeled lipids with $D \geq 0.4 \times 10^{-9}$ cm²/s, number of gold particles in parentheses.
‡ Mean ± SD, number of photobleaches in parentheses.
§ Used FRAP value for stationary cells treated with heparinase.
‖ From Lee et al., 1991.

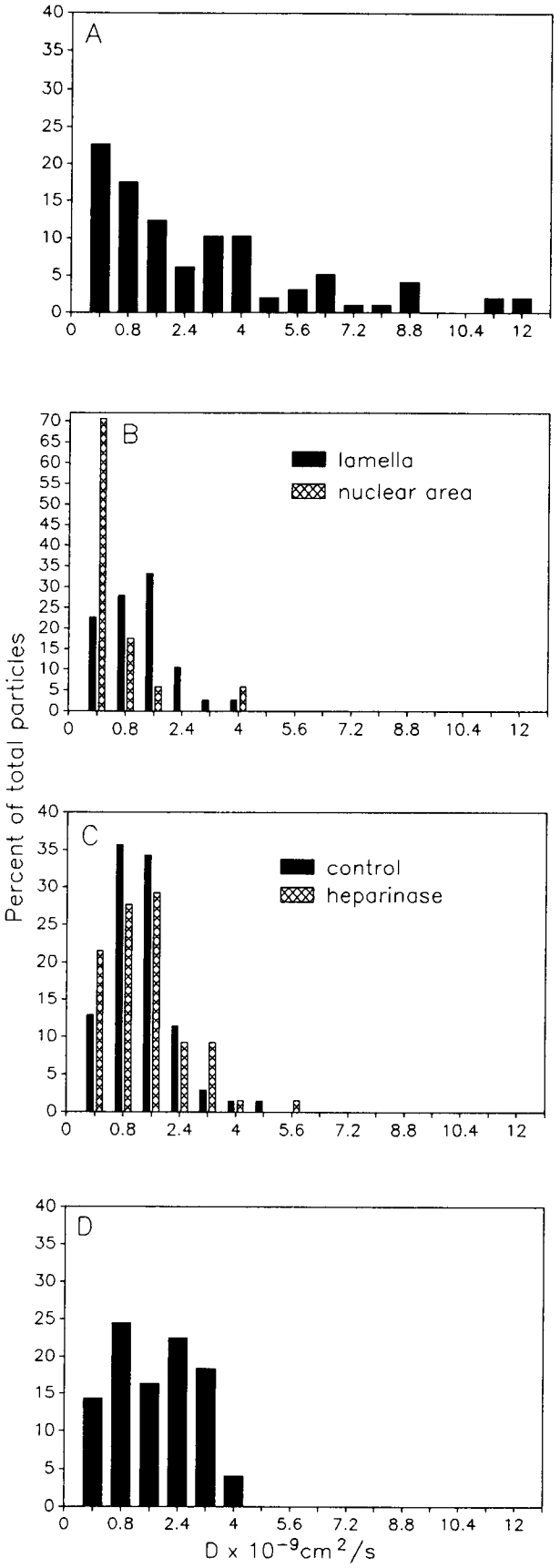

Figure 3. The distributions of D for individual gold-labeled lipids on the lamella of each cell type compared with the distribution found with the planar membrane (Lee et al., 1991). The numbers on the x axis indicate the upper limit of each interval. Note that there are several gold particles on the planar membrane with D above 5.6 × 10^{-9} cm^2/s, but there are none above this value for the untreated cells (also compare with Fig. 4). (*A*) Planar membrane, total of 75 particles, (*B*) fibroblasts, 75 particles on the lamella and 17 particles over the nuclear area, (*C*) PtK1 cells, 70 particles without and 65 particles with heparinase treatment and (*D*) fish scale cells, 49 particles.

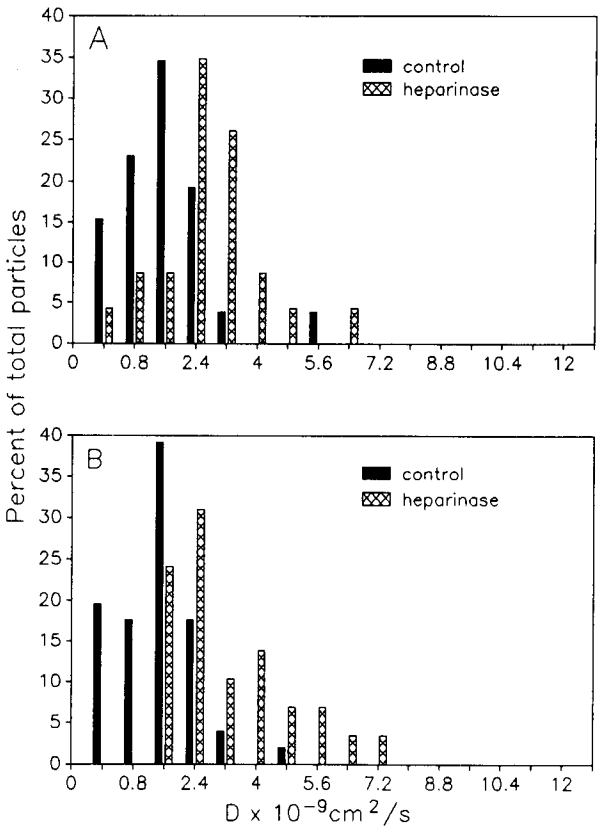

Figure 4. Comparison of the distributions of D for individual, multivalent gold-labeled lipids on stationary and crawling keratocytes, before and after enzyme treatment. Only the heparinase treatment has a distribution of D similar to that for the planar membrane (Fig. 3 *A*). (*A*) Stationary, 26 particles without and 22 particles with heparinase treatment; (*B*) crawling, 51 particles without and 29 particles with heparinase treatment.

for the gold labeled Fl-PE (D_G) was from 1.1 to 1.6 × 10^{-9} cm^2/s depending on cell type (Table I). This is lower than the average values of D for Fl-PE in the lamellar plasma membrane as measured with FRAP (D_F) (5.4 to 9.5 × 10^{-9} cm^2/s; and Table I). As can be seen in the table, D_G/D_F is, in general, only slightly smaller than that for the multivalent gold with the artificial planar membrane. Thus the lower D for the gold-labeled lipids, as compared to D_F, can be assumed to be partially due to the multivalency of the gold. However, 16% of the multivalent gold particles in the artificial planar membranes had a value for D > 6 × 10^{-9} cm^2/s (Fig. 3 *A*; Lee et al., 1991), but no control cells had any gold-labeled lipids which diffused as fast (distributions are shown in Figs. 3 and 4).

The lower range for D in the cells does not appear to be due to restriction of movement of the gold-labeled lipids to

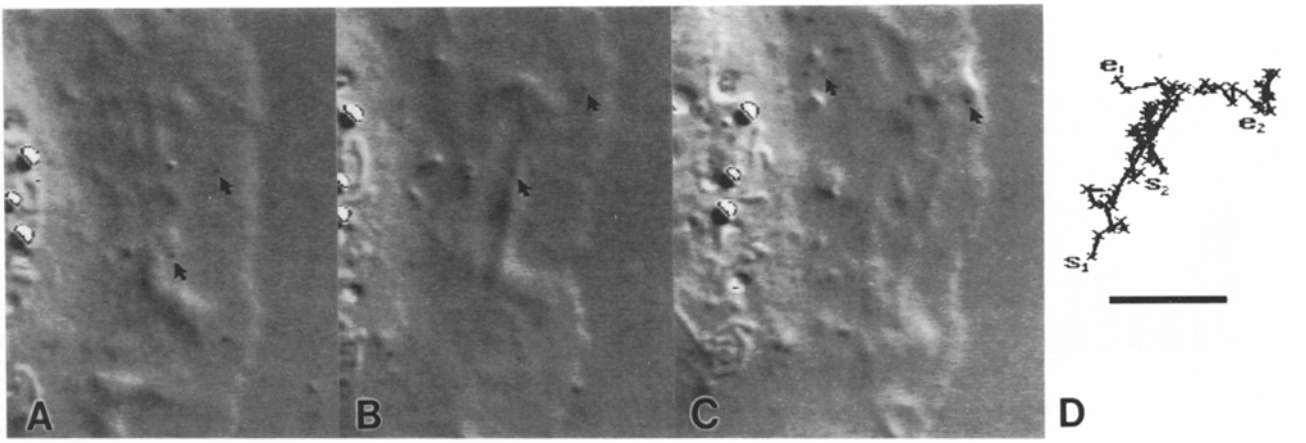

Figure 5. Gold-labeled lipids travel long distances on the cell surface of a crawling keratocyte. The random motion of the gold particles (*arrows*) is independent of cell locomotion. In these DIC images, the cell is crawling from left to right, but one particle moves roughly perpendicular to the direction of locomotion and then moves rearward. The other particle also moved perpendicular and then moved to the leading edge of the cell. It later moved away from the cell edge (not shown). (*A*) time 0, (*B*) 20 s, (*C*) 40 s, and (*D*) the trajectories (relative to the substrate) followed by the gold particles; (s_1 and s_2) starting positions; (e_1 and e_2) respective ending positions. X's indicate positions at 1-s intervals. Bar, 6 μm.

small corrals or domains since some gold particles had a net displacement of several microns (Fig. 5). The random, relatively unconfined nature of the movements of the gold-labeled lipids is further demonstrated by the MSD plots which approach linearity (Gross and Webb, 1988) when averaged for several trajectories (Fig. 6). Because detectable domain size is directly dependent on D for a given observation time (see below), the MSD has been averaged only for particles with a $D \geq 1.6 \times 10^{-9}$ cm²/s for the fibroblasts, PtK, and fish scale cells (Fig. 6 *A*). For the keratocytes (Fig. 6 *B*), all particles with $D \geq 1.3 \times 10^{-9}$ cm²/s were included in order to have enough data points to partially compensate for random variation. The slight bending of the MSD curve toward the time interval axis of some of the curves (e.g., Fig. 6 *B*) may be due to random variation (compare with Fig. 7 *F*). However, large domains or percolation of the gold-labeled lipids could also produce similar shaped curves (see below and the Discussion). When all particles with $D \geq 0.4 \times 10^{-9}$ cm²/s were included, the average MSD plots were linear (not shown).

The effect of restricted diffusion on the MSD plot can best be understood by using computer simulations of confined diffusion. In a somewhat simplistic model, we have simulated Brownian motion in circular domains with an impenetrable boundary. If the diffusion coefficient, domain size, and observation time are matched so that the diffusants are likely to sample the domain wall for some portion of their trajectory, then the MSD plots will bend toward the x axis (Fig. 7, *A* and *D*). A particle with a large D in a small domain maximizes this effect, but a consistent bending of the averaged MSD plots occurs even when the barrier is encountered for only small portions of the trajectories (Fig. 7, *B* and *E*). If the domain is large and D is small, the diffusants may or may not sample the domain boundary within the observation time (Fig. 7 *C*). In this case, an encounter with the boundary depends on where in the domain the diffusant begins its trajectory. Thus in Fig. 7 *F*, some of the averaged MSD plots show some bending whereas others do not.

Because the maximum domain size detectable is dependent on the diffusion coefficient and the observation time, domains with a diameter of ~6 μm or larger would not have been reliably detected in our usual observation time of 7 s. Based on the simulations of confined diffusion, a domain of 5 μm (not shown) would give average MSD plots similar to those observed with the untreated keratocytes (Fig. 6 *B*). However, when individual gold-labeled lipids were observed for longer periods of time, their net displacement was on the order of 7 to 9 μm in 40 s (Fig. 5) suggesting that, at least in some instances, longer excursions are possible.

A possible reason for the gold-labeled lipids on cells having a lower average and lower maximum D value than for the planar membranes is that cells have a pericellular matrix which could impede the movement of the gold-labeled lipids. That the cells examined in this study have such a matrix is demonstrated by the particle exclusion assay and by the electron micrographs shown in Fig. 8. The pericellular matrix appears as a clear area between the plasma membrane and the red blood cells in Fig. 8, *A–D*. The extent of the matrix was greater for the fibroblasts than for the PtK cells and the keratocytes. In the electron micrograph of the C3H fibroblast (Fig. 8 *F*), the pericellular matrix can be seen to include both putative proteins projecting from the plasma membrane and a fine meshwork which extends from the cell surface outward several microns. In the electron micrograph of a keratocyte (Fig. 8 *G*), the pericellular matrix appears as a patchy, fuzzy material. For either cell type, the gold particles attached to lipid molecules in the plasma membrane (Fig. 8 *E*) would have to move through this matrix.

To test the possibility that the pericellular matrix slowed lateral motion of gold-labeled lipids, keratocytes were treated with heparinase, an enzyme which degrades components of the pericellular matrix. Heparinase treatment of keratocytes resulted in a twofold increase in the average D_G ($P < 0.0001$ when compared to control cells using analysis of variance), but had no effect on D_F (Table I). For the heparinase-treated keratocytes, there were 6 out of 51 particles with D greater than 4.8×10^{-9} cm²/s (Fig. 4). In contrast, out of a total of 224 particles (with $D \geq 4 \times 10^{-10}$

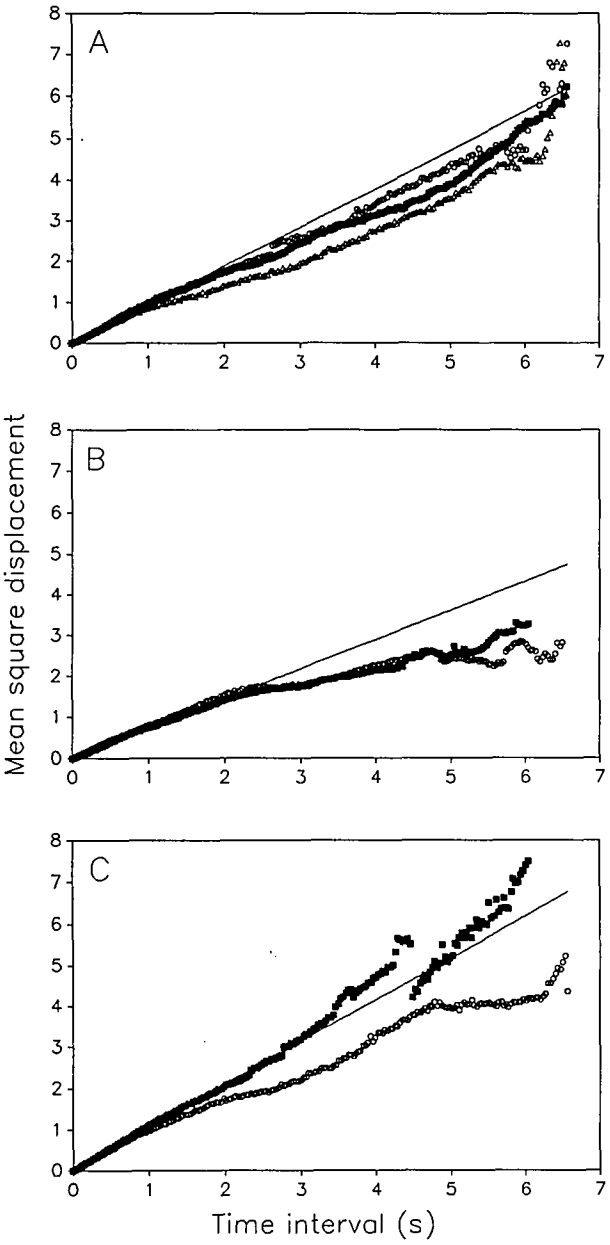

Figure 6. Averaged MSD plots for gold-labeled lipids demonstrate that the overall pattern of movement is random motion as opposed to corralled or transported. MSD is in square microns. (*A*) The plots were averaged for particles with D≥ 1.6 × 10^{-9} cm^2/s; (○) C3H fibroblasts, 12 gold particles; (■) PtK1 cells, 12 gold particles, and (△) fish scale fibroblasts (third passage), 21 gold particles. On keratocytes, the plots were averaged for particles with D ≥ 1.3 × 10^{-9} cm^2/s; (*B*) (■) crawling, 18 gold particles, (○) stationary, nine gold particles; and (*C*) (■) crawling after heparinase treatment, 25 gold particles, (○) stationary after heparinase treatment, 22 gold particles. The straight lines were computed from the equation MSD = 4Dt, where D was calculated from the slope of the averaged plots for the short time intervals. For the crawling cells, the MSD for each trajectory was corrected for the cell's displacement relative to the substrate to which the cell was attached (see Materials and Methods for details). The break in the curve for the heparinase treated cells is due to an incomplete data set for a particularly fast moving particle which could not be tracked for a full 200 frames.

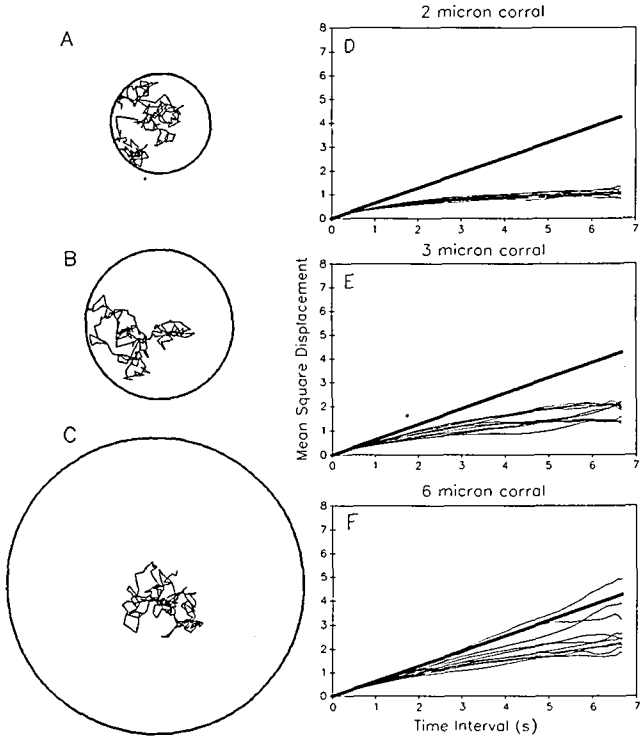

Figure 7. Computer simulations of random motion inside a circular corral give an indication of what size domain is detectable under our experimental conditions. The perimeter of the circle acts as a non-reflective, impenetrable barrier in that motion stops until a direction away from the barrier is randomly generated. The random walks were generated with D = 1.6 × 10^{-9} cm^2/s. Each trajectory is the equivalent of 200 images collected at video rate. The corral diameters are (*A*) 2 μm, (*B*) 3 μm, and (*C*) 6 μm. To demonstrate the effect of random variation on the linearity and shape of the MSD plots, ten plots, representing a total of 200 trajectories, are shown for each corral size. Each MSD plot was averaged for 20 trajectories. The bold, straight lines were computed from the equation MSD = 4Dt, where D = 1.6 × 10^{-9} cm^2/s. When there is significant interaction of the trajectory with the barrier as in *A* the corresponding MSD plots (*D*) are bent toward the time-interval axis at a fairly short time interval. When the interaction is of relatively short duration (*B* and *C*), the MSD plots (*E* and *F*) are bent after longer time intervals. In *C* the domain is so large that only some of the trajectories interact with the boundary resulting in greater variability in the averaged MSD plots (*F*).

cm^2/s) tracked on all of the untreated cells, only one particle had a D greater than 4.8 × 10^{-9} cm^2/s (Figs. 3 and 4). Heparinase treatment of PtK cells produced a slight but insignificant increase in D (Table I; and Fig. 3).

The diffusion of the Fl-PE was found to be reduced in the plasma membrane over the nuclear area compared to over the lamella in C3H fibroblasts. This was found for gold Fl-PE where the average D for a few particles with D ≥ 4 × 10^{-10} cm^2/s was not slower but there was a much greater percentage of particles with D < 4 × 10^{-10} cm^2/s (Table I; and Fig. 3 *B*). The MSD plots for the gold particle trajectories (not shown) were linear indicating that the lateral movement of the gold particles was slower but not restricted. The FRAP measurements also revealed a significant difference ($P < 0.05$, *t*-test) in D for Fl-PE, D = 5.4 × 10^{-9} cm^2/s for the lamella compared to 3.8 × 10^{-9} cm^2/s for the plasma mem-

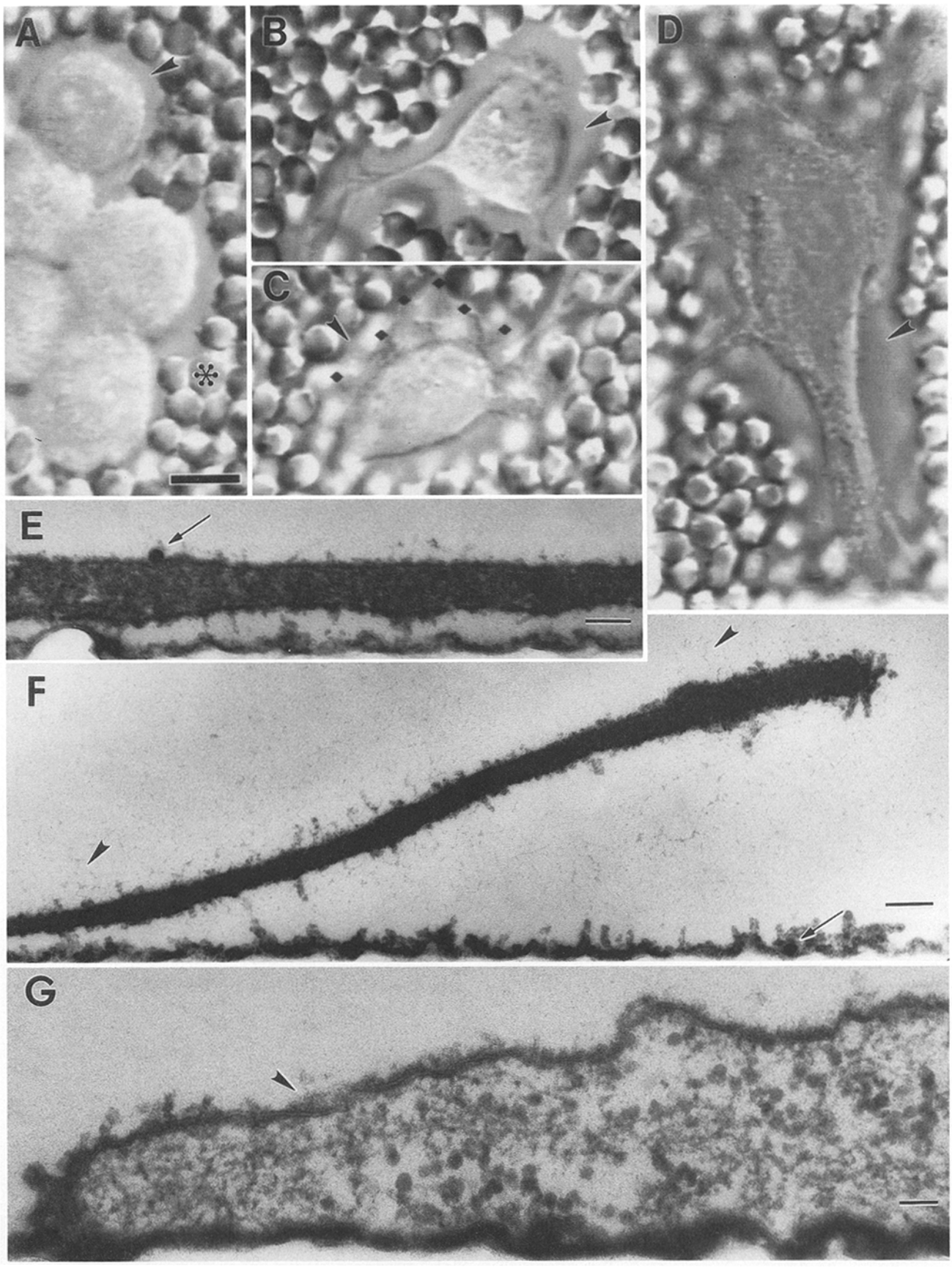
A
B
C
D
E
F
G

brane over the nucleus. Under the nucleus, the plasma membrane had a D similar to that for the lamella (data not shown). As a control we used FRAP to measure the diffusion of DiI, a fluorescent lipid probe with a minimal head group. DiI had the same average D for all areas. Thus the lower D for the plasma membrane over the nucleus is not due to a rougher membrane topography, increased bulk membrane viscosity, or to an artifact in the FRAP measurements.

We found no indication of membrane flow during cell locomotion. The gold Fl-PE moved in random patterns independent of the direction of cell locomotion (Fig. 5). The velocity-corrected MSD plots for the crawling keratocytes are similar to the MSD plots for the stationary keratocytes (Fig. 6 *B*). When averaged over all the tracks with $D > 4 \times 10^{-10}$ cm²/s, both plots are nearly linear with no upward deflection. An upward deflection of the averaged MSD plot would indicate membrane flow. The velocity correction (see Materials and Methods) was necessary as our analysis method only looks at the particle in reference to the substrate to which the cell is attached. Without the velocity corrections, the average MSD plot curved upward (not shown) consistent with the membrane moving as a unit with the cell. Since the average D of the gold Fl-PE is fairly high (1.3×10^{-9} cm²/s), Brownian motion could mask detection of a very slow membrane flow (Qian et al., 1991).

In the experiments with the artificial planar membranes, a major difference was found in the diffusion of multivalent and paucivalent gold probes (in this context, valency refers to the number of fluorescein antibodies per gold particle) (Lee et al., 1991). Because of poor binding of the paucivalent gold anti-Fl probe (the level was barely above background), sufficient data is not available for a conclusive statement on the difference in paucivalent and multivalent gold probes on the cells. Preliminary data indicate that, for the cells, there was no difference in paucivalent and multivalent probes. This may be due to the pericellular matrix limiting diffusion and thus obscuring any effects due to the increased valency of the gold probe.

Discussion

We have shown that gold-tagged Fl-PE can diffuse freely in the plasma membrane of spreading and locomoting cells. Thus gold Fl-PE does not appear to be confined to moving within small regions of the outer leaflet of the plasma membrane bilayer. The free movement of the lipid with a gold tag, which projects 30 to 40 nm above the lipid bilayer, indicates that there are few, if any, barriers in the pericellular matrix in this 40-nm thick zone above the plasma membrane.

Lateral Heterogeneity in the Bilayer

With respect to heterogeneity, within the plane of the membrane, the term "domain" can refer to either a barrier-free enrichment of a molecular species in the membrane or to the confinement of a molecule(s) to a given region by barriers (Glaser, 1982; Edidin, 1992). Both mechanisms of regionalization should be detected by nanovid microscopy using gold-labeled lipids. Using nanovid microscopy, DeBrabander et al. (1991) reported restricted motion for the lipid-linked protein, Thy-1. However, no such confinement was reported by the gold probe when attached to a lipid analog.

Our results are in contrast to several reports in the literature. Rodgers and Glaser (1991) have shown, using digitized fluorescence microscopy of phospholipids labeled on their acyl chains with either the NBD or dansyl groups, that regions exist in the plasma membrane of red blood cells that are enriched in specific lipids. Lipid domains in the plasma membrane of sperm have been demonstrated by differential scanning calorimetry (Wolf et al., 1990). Yechiel and Edidin (1987) concluded that lipid domains exist in fibroblasts based on their FRAP experiments using an acyl-labeled NBD-phosphatidylcholine. On the other hand, Metcalf et al. (1986) found no indication of lipid domains in 3T3 fibroblasts when performing FRAP measurements using either NBD conjugated to the head group of phosphatidylethanolamine or acyl-NBD phosphatidylcholine.

While the above results are apparently at odds, the studies differ in important variables such as the structure of the lipid probe, its concentration in the membrane, the temperature during labeling and measurement, and the cell type. For instance, the sperm plasma membrane is exceptional because of its unique lipid composition (Wolf et al., 1990). Whether a probe's structure alters the natural physiological state of the membrane or affects its ability to report accurately on membrane structure and dynamics is still an open question.

With respect to our experiments in particular, the Fl-PE appeared uniformly incorporated in the plasma membrane on the lamella of all cells examined (not shown), and there did not appear to be discrete regions on a given cell's lamella where the gold-labeled lipids diffused in a confined fashion; however, based on the Yechiel and Edidin (1987) experiments, we might have expected lipid domains to exist in the lamellar regions. We did not examine the plasma membrane above the peri-nuclear region because of confusion of the gold particles with underlying organelles. Thus, either areas of pronounced lipid enrichment do not exist in these cells or our probe fails to be restricted by these putative regions. Some fluid domains may be head group specific (Rodgers and Glaser, 1991) in which case foreign probes, such as dil

Figure 8. All of the cells used in this study had a pericellular matrix as is shown by the particle exclusion assay (*A–D*) and as shown in electron micrographs of cells sectioned perpendicular to the substrate (*E–G*). Cells were used 2 d after subculturing and had a similar morphology as the cells used for gold particle tracking. For the particle exclusion assay, fixed red blood cells in PBS are layered over living cells attached to a substrate. The absence of divalent cations causes the cells to round resulting in easier visualization of the pericellular matrix (*arrowheads*) which can be seen as a clear area between the plasma membrane and the red blood cells. (*A*) Cluster of PtK cells, the asterisk indicates a red blood cell; (*B*) fish scale fibroblast; (*C*) keratocyte, the diamonds indicate the edge of the lamella; (*D*) C3H fibroblast. For the electron micrographs, preservation of the pericellular matrix was enhanced by adding Alcian blue to the fixative. Arrows indicate gold particles (*E* and *F*). The figures demonstrate that many plasma membrane-associated matrix components project above the gold particles (*E*). In the section of a C3H fibroblast lamella (*F*), a fine meshwork extending out from the plasma membrane (*arrowheads*) appears associated with the numerous denser structures projecting out from the plasma membrane. The lamella of a keratocyte (*G*) has a more amorphous pericellular matrix that appears as fuzzy patches (*arrowhead*). Bars: (*A*) 10 μm; (*E* and *F*) 0.1 μm; (*G*) 0.05 μm.

or probes with altered head groups such as gold Fl-PE, would fail to partition into them. However, if the gold Fl-PE was excluded from some regions, this would also cause the averaged MSD plot to bend toward the time-interval (x) axis. This is evident in Fig. 7, *B* and *D* of the computer simulation of Brownian motion. In the three micron corral, the diffusant only samples a small portion of the corral boundary, but the MSD plot is still deflected downward. Barriers would produce a similar effect (Saxton, 1989).

In principle, actual barriers to free diffusion of the gold-labeled lipids could exist either in the plane of the membrane or in the pericellular matrix. The presence of barriers in either place would place restrictions on free diffusion resulting in what has been termed "percolative" diffusion (for example, see Saxton, 1989). If the barriers are so abundant as to prevent long range diffusion, the diffusant will appear to be in a corral or domain. When the barriers are partially opened or removed, long range but impeded, diffusion occurs. As with corralled diffusion, MSD plots associated with percolative diffusion are bent toward the time interval (x) axis with the degree of bending due to the number of closed barriers (Saxton, 1989). With increased barriers, movement is restricted to a smaller area and the MSD plot becomes the same as for diffusion in a small corral. The average MSD plots for the untreated keratocytes (Fig. 6 *B*) could be interpreted as either percolative diffusion or corralled diffusion in a 5 μm or larger domain.

Our results are consistent with those of Edidin et al. (1991) who used a laser trap to move either membrane-spanning or lipid-linked gold-labeled proteins in the plane of the plasma membrane. The lipid-linked protein labeled with gold is somewhat analagous to our gold Fl-PE probe. They found that, at 34°C, a GPI-anchored molecule could be moved 8.4 μm on the average without encountering a barrier and some labeled particles could be moved considerably longer distances. Based on our computer simulations of random motion with barrier-bounded domains, we would not be able to detect a domain as large as 6 μm with statistical certainty in the time frame of most of our experiments (7 s). Therefore, we conclude that if there are domains limiting the diffusion of Fl-PE, most are larger than 5 μm in diameter.

That barriers to diffusion of gold Fl-PE were not created by pericellular matrix components on the cells examined is not so surprising upon reflection. Filamentous structures appear to be lacking in the extracellular matrix over the lamella since fibronectin and heparan sulfate proteoglycans are not ordered into fibrils on the dorsal surface of the lamella of spreading cells (unpublished observations). However, the cells used in this study had an amorphous pericellular matrix surrounding the cell as determined by the particle exclusion assay (Clarris and Fraser, 1968; Underhill and Toole, 1982). That there was a pericellular matrix on the lamellar region was shown by EM.

Viscosity of the Pericellular Matrix

Information on the viscosity of this matrix near the plasma membrane can be obtained by comparing the magnitude of the D_G value for the gold-Fl-PE with that of D_F obtained by FRAP. While a significant portion of the reduction in the D_G of the gold-Fl-PE relative to the D_F for Fl-PE is due to the multivalent nature of the gold probe, this study suggests that the viscosity of the pericellular matrix was also a factor. This was shown by the significant increase in D_G after heparinase treatment.

We cannot give a precise value for the viscosity of the pericellular matrix based on the D of gold Fl-PE as current theoretical models do not adequately describe a situation in which two different sized, but linked moieties, diffuse in adjacent layers of different viscosity. However, if we assume that the plasma membrane and the pericellular matrix are separate layers whose components move independently, we can compute an approximate viscosity from the frictional coefficients of the different moieties. The frictional coefficients, f, can be calculated from the measured diffusion coefficients using the Einstein relationship:

$$f = kT/D \tag{2}$$

where k is the Boltzman constant and T is the absolute temperature. We can write, as previously described (Zhang et al., 1991):

$$f_{total} = f_{gold} + f_{lipid} \tag{3}$$

where f_{gold} and f_{lipid} are the frictional coefficients of the antibody-coated gold and the anchoring Fl-PE, respectively. The total frictional coefficient, f_{total}, can be calculated from D_G, and f_{lipid} can be calculated from D_F using equation (2). D_F may need to be adjusted since the average D_G was lower than D_F in the planar membrane where there was no pericellular matrix (Lee et al., 1991). The pericellular matrix viscosity can be computed from f_{gold} using the Stokes law:

$$f_{gold} = 6\pi\eta a \tag{4}$$

where η is the viscosity of the matrix and a is the radius of the antibody coated gold particle, which we approximate to be 20 nm. (Strictly speaking, of course, the Stokes formula is not applicable because we have pseudo two-dimensional diffusion of the gold through a thin slab of viscous pericellular matrix material adjacent to the plasma membrane.) For the untreated cells, the apparent pericellular matrix viscosity values ranged from 0.56 to 0.86 P with no correction of D_F and from 0.46 to 0.73 P with D_F corrected by the ratio of D_G to D_F seen with the paucivalent gold in the planar membrane. (D_G/D_F for the multivalent gold in the planar membrane could not be used as this adjustment produced a negative frictional coefficient.) For the heparinase-treated keratocytes, matrix viscosity was 0.23 and 0.11 P for no correction and corrected, respectively. Thus the viscosity of the pericellular matrix is significantly less than that of the plasma membrane (usually considered to be ~1.0 to 10 P; Cherry, 1979) and is much greater than water (0.01 P). For comparison, the viscosity of 60% sucrose at 25°C is 0.44 P (Dean, 1973).

Diffusion in the Plasma Membrane over the Nuclear Area

The plasma membrane over the nucleus in fibroblasts had a significantly lower D_F and a larger proportion of slow moving gold-tagged lipids. There are two possible reasons for this: (*a*) the pericellular matrix has a higher viscosity; or (*b*) there is a greater interaction of the Fl-PE with some other component in the plasma membrane over the nucleus. The

latter possibility would suggest that this whole area could be considered as a domain, a domain that is larger than we can detect with the gold-labeled lipids. The first possibility can neither be ruled out nor accepted at this time but could be tested with an enzyme treatment to remove the pericellular matrix on fibroblasts. (Heparinase treatment, in our hands, was not effective on these cells.)

Now that we have shown that gold-labeled lipids can freely diffuse in the plasma membrane of living cells, further work can be undertaken to determine if an increased time in culture will produce a more restrictive pericellular matrix. Other cell morphologies, such as cells with pronounced stress fibers that have ordered fibronectin and heparin sulfate proteoglycan fibrils (Woods et al., 1984), may show a greater reduction in the free diffusion of the gold Fl-PE. In fact, preliminary data on a C3H fibroblast with prominent stress fibers indicate that the gold Fl-PE has a lower average and lower maximum D_G than in spreading cells. However, the average MSD plots were also linear indicating that barriers to free diffusion were not present.

In conclusion, by using gold-labeled lipids, we have shown that a truly novel aspect of nanovid microscopy is that it offers the capability to probe the structure of the adjacent pericellular matrix as well as molecular mobility and spatial arrangements in the plasma membrane.

We express our appreciation to Drs. Brad Chazotte and Evan Evans for helpful discussions, to Mrs. Victoria Madden and Dr. Joe Costello for help with the EM, to Dr. Robert Bagnell for his help in the use of his photographic enlarger, and to Ms. Tena Rosser for help in data analysis.

This research was supported by National Institutes of Health grants GM 41402 and GM 13167-02.

Received for publication 8 May 1992 and in revised form 11 August 1992.

References

Behnke, O., and T. Zelander. 1970. Preservation of intercellular substances by the cationic dye Alcian Blue in preparative procedures for electron microscopy. *J. Ultrastruct. Res.* 31:424–438.

Billings-Gagliardi, S., S. W. Pockwinse, and G. B. Schneider. 1981. Surface coats on human lymphocytes: freeze drying and staining with cations. *Am. J. Anat.* 154:267–276.

Cherry, R. J. 1979. Rotational and lateral diffusion of membrane proteins. *Biochim. Biophys. Acta.* 559:289–327.

Clarris, B. J., and J. R. E. Fraser. 1968. On the pericellular zone of some mammalian cells *in vitro*. *Exp. Cell Res.* 49:181–193.

Curtain, C. C., L. M. Gordon, and R. C. Aloia. 1988. Lipid domains in biological membranes: conceptual development and significance. *In* Lipid Domains and the Relationship to Membrane Function. R. C. Aloia, C. C. Curtain, and L. M. Gordon, editors. Alan R. Liss, Inc., New York. 1–15.

Dean, J. A. 1973. Lange's Handbook of Chemistry Eleventh Ed., McGraw-Hill, New York. 10–287.

DeBrabander, M., R. Nuydens, A. Ishihara, B. Holifield, K. Jacobson, and H. Geerts. 1991. Lateral diffusion and retrograde movements of individual cell surface components on single motile cells observed with nanovid microscopy. *J. Cell Biol.* 112:111–124.

Edidin, M. 1990. The super-ordered fluid: a domain model of cell surface membranes. *In* Biophysics of the Cell Surface. Vol. 5. R. Glaser and D. Gingell, editors. Springer-Verlag, New York. 51–59.

Edidin, M. 1992. The variety of cell surface membrane domains. *Commun. Mol. Cell. Biophys.* 8:73–82.

Edidin, M., and I. Stroynowski. 1991. Differences between the lateral organization of conventional and inositol phospholipid-anchored membrane proteins. A further definition of micrometer scale membrane domains. *J. Cell Biol.* 112:1143–1150.

Edidin, M., S. C. Kuo, and M. P. Sheetz. 1991. Lateral movements of membrane glycoproteins restricted by dynamic cytoplasmic barriers. *Science (Wash. DC).* 254:1379–1382.

Geerts, H., M. DeBrabander, R. Nuydens, S. Geuens, M. Moeremans, J. DeMey, and P. Hollenbeck. 1987. Nanovid tracking: a new automatic method for the study of mobility in living cells based in colloidal gold and video microscopy. *Biophys. J.* 52:775–782.

Glaser, M. 1992. Characterization and formation of lipid domains in vesicles and erythrocyte membranes. *Commun. Mol. Cell. Biophys.* 8:37–51.

Gross, D. J. and W. W. Webb. 1988. Cell surface clustering and mobility of the liganded LDL receptor measured by digital video fluorescence microscopy. *In* Spectroscopic Membrane Probes. Vol. II. L. M. Loew, editor. CRC Press, Inc., Boca Raton, FL. 19–45.

Hartwig, J. H., D. A. Ausiello, and D. Brown. 1987. Vasopressin-induced changes in the three-dimensional structure of toad bladder apical surface. *Am. J. Physiol.* 253:C707–C720.

Hedman, K., S. Johansson, T. Vartio, L. Kjellen, A. Vaheri, and M. Hook. 1982. Structure of the pericellular matrix: association of heparan and chondroitin sulfates with fibronectin-procollagen fibers. *Cell.* 28:663–671.

Hunziker, E. B., and R. K. Schenk. 1987. Structural organization of proteoglycans in cartilage. *In* Biology of Proteoglycans. T. N. Wight and R. P. Mecham, editors. Academic Press, Orlando, FL. 155–185.

Hunziker, E. B., W. Herrmann, and R. F. Schenk. 1983. Ruthenium hexamine trichloride (RHT)-mediated interaction between plasmalemmal components and pericellular matrix. *J. Histochem. Cytochem.* 31:717–727.

Ito, S. 1974. Form and function of the glycocalyx on free cell surfaces. *Phil. Trans. R. Soc. Lond. B.* 268:55–66.

Kjellan, L., and U. Lindahl. 1991. Proteoglycans: structures and interaction. *Annu. Rev. Biochem.* 60:443–475.

Knudson, W., and C. B. Knudson. 1991. Assembly of a chondrocyte-like pericellular matrix on non-chondrogenic cells. Role of the cell surface hyaluronan receptors in the assembly of a pericellular matrix. *J. Cell Sci.* 99:227–235.

Kucik, D. F., E. L. Elson, and M. P. Sheetz. 1990. Cell migration does not produce membrane flow. *J. Cell Biol.* 111:1617–1622.

Lee, G. M., A. Ishihara, and K. A. Jacobson. 1991. Direct observation of Brownian motion of lipids in a membrane. *Proc. Natl. Acad. Sci. USA.* 88:6274–6278.

Metcalf, T. N., III, J. L. Wang, and M. Schindler. 1986. Lateral diffusion of phospholipids in the plasma membrane of soybean protoplasts: evidence for membrane lipid domains. *Proc. Natl. Acad. Sci. USA.* 83:95–99.

Qian, H., M. P. Sheetz. and E. L. Elson. 1991. Single particle tracking analysis of diffusion and flow in two-dimensional systems. *Biophys. J.* 60:910–921.

Rodgers, W., and M. Glaser. 1991. Characterization of lipid domains in erythrocyte membranes. *Proc. Natl. Acad. Sci. USA.* 88:1364–1368.

Saxton, M. J. 1989. The spectrin network as a barrier to lateral diffusion in erythrocytes A percolation analysis. *Biophys. J.* 55:21–28.

Toole, B. P. 1991. Proteoglycans and hyaluronan in morphogenesis and differentiation. *In* Cell Biology of Extracellular Matrix. 2nd ed. E. D. Hay, editor. Plenum Publishing Corp. New York. 305–341.

Underhill, C. B., and B. P. Toole. 1982. Transformation-dependent loss of the hyaluronate-containing coats of cultured cells. *J. Cell. Physiol.* 110: 123–128.

Van den Pol, A. N., M. Ellisman, and T. Deerinck. 1989. Plasma membrane localization of proteins with gold immunocytochemistry. *In* Colloidal Gold: Principles, Methods and Applications. Vol. 1. M. A. Hayat, editor. Academic Press, San Diego, CA. 452–487.

Viitala, J., and J. Jarnefelt. 1985. The red cell surface revisited. *Trends Biochem. Sci.* Oct. 392–395.

Wade, J. B., and R. A. Coleman. 1989. Direct visualization of the interrelationship between intramembrane and extracellular structures. *Proc. Natl. Acad. Sci. USA.* 86:2723–2727.

Wolf, D. E., V. M. Maynard, C. A. McKinnon, and D. L. Melchior. 1990. Lipid domains in the ram sperm plasma membrane demonstrated by differential scanning calorimetry. *Proc. Natl. Acad. Sci. USA.* 87:6893–6896.

Woods, A., M. Hook, L. Kjellen, C. G. Smith, and D. A. Rees. 1984. Relationship of heparan sulfate proteoglycans to the cytoskeleton and extracellular matrix of cultured cells. *J. Cell Biol.* 99:1743–1753.

Yechiel, E., and M. Edidin. 1987. Micrometer scale domains in fibroblast plasma membranes. *J. Cell Biol.* 105:755–760.

Zhang, F., B. Crise, B. Su, Y. Hou, J. K. Rose, A. Bothwell, and K. Jacobson. 1991. Lateral diffusion of membrane-spanning and glycosylphosphatidylinositol-linked proteins: toward establishing rules governing the lateral mobility of membrane proteins. *J. Cell Biol.* 115:75–84.